Chapter 4
Application to Life Sciences

Life is when structure acts as a function—is one of the many answers given to the everlasting question "What is life?".

The evolution of such functions of living beings in nature constitutes a vast group of complex dynamical systems. In order to maintain their functioning and activity, many of the processes tend to reach a balance between energy inflow and dissipated energy—forming a periodic i.e. oscillatory process.

But how well is the balance maintained throughout the system's evolution? In general, the biological systems are not isolated and often they are thermodynamically open. This causes a different type of energy exchange, in addition to the dissipated energy needed to maintained the basic functioning of the system. In other words, the system dynamics are no longer autonomic, and other processes contribute to its time-evolution. Within the same environment (for example—the human body) the sources of external influence are often known and closely related processes—which can be regarded as deterministic. The effect of the external dynamics can cause the intrinsic parameters, the interactions, or even functional dependencies to vary with time.

The following chapter focuses on the discussion on effects from external influences on human physiology. The underlying physiological systems are considered to be oscillatory processes and their dynamical characterization is studied. One of the main objectives was to investigate some of the physiological mechanisms with respect to deterministic non-autonomous perturbations. The latter involved physiological measurements while the respiration frequency was varied in time. Another issue discussed is the dynamical characterization of blood flow oscillations and their transient effect when subject to external perturbations. Several methodological issues regarding the time-varying analysis and estimates are also discussed. By exploiting the measured time-series, the analysis (i.e. the inverse problem approach) employs many of the theoretical and methodological concepts discussed in the previous chapters.

T. Stankovski, *Tackling the Inverse Problem for Non-Autonomous Systems*,
Springer Theses, DOI: 10.1007/978-3-319-00753-3_4,

4.1 A Short Physiological Background

This section lays down the necessary human physiological background that any non-biological scientist can find useful for the remaining of the chapter. For a more comprehensive physiological background one can refer to [1–4].

4.1.1 Cardiovascular System

The cardiovascular system forms a blood distribution network for transport of nutrients, gases and wastes to and from cells. It consists of three principle components: the heart, blood vessels and blood. According to cardiovascular functioning the system can be divided into pulmonary and systemic (peripheral) circulation. The pulmonary circulation connects the lungs where the blood is oxygenated, while the systemic supplies the rest of the body with the oxygenated blood.

The heart is a muscular organ, which forms two separate (right and left) pumps, each composed of atrium and ventricle chambers. The function of the right side is to collect the de-oxygenated blood in the right atrium and to pump it through the right ventricle to the lungs where it is oxygenated. The oxygenated blood is collected in the left atrium and pumped through the left ventricle to the rest of the body. The pumping action of the heart is based on a rhythmic *oscillatory* sequence of relaxation (diastole) and contraction (systole) procedures. The heartbeat coordination is tightly controlled by the sinoatrial node which acts as a pacemaker that determines the heart rate. The cardiac output i.e. the amount of blood pumped for a resting human subject, is about 5 l in 1 min.

Depending on the blood flow direction, two types of vessels exist: arteries and veins. The arteries take the blood away from the heart, and veins bring the blood back to the heart. Due to the high pressure, the arteries have strong vascular walls and blood flows rapidly to the tissues. At the endings of the arterial system are arterioles acting as control valves through which blood is released to the capillaries. The capillaries then allow the actual exchange substances between the blood and the surrounding tissue. The walls of both arteries and capillaries is lined by a thin layer of endothelia cells which cause the smooth muscles to constrict or relax, contributing to the regulation of the vascular tone. The veins transport the blood from the capillaries (through venules) to the heart, and serve as a reservoir of blood. Due to the low pressure, the venous walls are thin.

The blood is a special fluid with the main function of conveying substances within the body, such as gases (oxygen, carbon-dioxide), hormones, vitamins and enzymes. It is composed of a liquid, called blood plasma, and blood cells suspended within the plasma. An average human subject has around 5 l of blood, which accounts for about 6–8 % of their body weight.

4.1.2 Respiratory System

The respiratory system introduces respiratory gases to the interior of the body and performs gas exchange. It includes the airways, lungs, and the respiratory muscles. Molecules of oxygen and carbon dioxide are passively exchanged by diffusion between the gaseous external environment and the blood. This exchange process occurs in the alveolar region of the lungs. The respiration process is an oscillatory cycle composed of two sub-processes: inspiration and expiration. Expiration is the movement of air out of the bronchial tubes, through the airways to the external environment during breathing, while inspiration is the movement of air from the external environment through the air ways, and into the alveoli. The way in which the respiratory system works closely in concert with a circulatory system to carry gases to and from the tissues—means it is often considered to be part of the cardiovascular system.

4.1.3 Sympathetic Nervous System

The sympathetic nervous system is a part of autonomic nervous system (along with enteric and parasympathetic) which mainly controls involuntary internal processes. The sympathetic nervous system prepares the body for responses to stressful challenges, allowing sudden strenuous exercise and increased vigilance. Stress is thought to counteract the parasympathetic system, which generally works to promote maintenance of the body at rest.

The sympathetic nervous system is responsible for up- and down-regulating many homeostatic mechanisms in living organisms. Fibers from the sympathetic system innervate tissues in almost every organ system, providing at least some regulatory function to things as diverse as blood flow control, thermoregulation, gut motility, and urinary output. It is perhaps best known for mediating the neuronal and hormonal stress response, commonly known as the fight-or-flight response. This acts primarily on the cardiovascular system and is mediated directly via impulses transmitted through the sympathetic nervous system and indirectly via catecholamines secreted from the adrenal medulla.

Messages travel through the sympathetic nervous system in a bidirectional flow. Efferent messages can trigger changes in different parts of the body simultaneously, such as the acceleration of the heart rate; widening of the bronchial passages; reducing the motility (movement) of the large intestine or the constriction of blood vessels. Afferent messages carry sensations such as heat, cold, or pain.

4.1.4 Oscillatory Processes in the Cardiovascular System

The functioning of cardiovascular system is characterized by several oscillatory processes [3–5]. They are responsible for many of the modulations observed in the blood flow and the heart rate variability signals. Each of the oscillating processes has

Table 4.1 The frequency intervals for the distinctive oscillatory processes determined from human blood flow, and their physiological origin

Interval	Frequency (Hz)	Physiological origin
I	0.6–2	Cardiac
II	0.145–0.6	Respiratory
III	0.052–0.145	Myogenic
IV	0.021–0.052	Neurogenic
V	0.0095–0.021	Endothelial metabolic
VI	0.005–0.0095	Endothelial

a characteristic period and is well defined in a certain frequency interval (summarized in Table 4.1). Each also has a physiological interpretation, which is described in the following:

I The frequency interval around 1 Hz corresponds to cardiac oscillatory activity. It describes the periodicity for the functioning (pumping) of the heart.

II The oscillatory component around 0.2 Hz describes the respiratory activity and the periodicity associated with the breathing process that supplies the body with oxygenated blood.

III Around 0.1 Hz, corresponds to myogenic activity. The vessels are able to help control blood flow via a mechanism known as myogenic autoregulation. The vascular smooth muscles contract in response to an increase of intravascular pressure, and relax in response to a decrease of pressure.

IV The periodicity around 0.04 Hz originates from the activity of the autonomic nervous system on the heart, lungs and vessels. The nerves cause the release of substances that affect the activities of smooth muscles, leading in turn to changes in the vessels' radii and resistance, which allows vasoconstriction to take place.

V The oscillations around 0.01 Hz, correspond to nitric oxide (NO)-related endothelial activity. The layer of endothelial cells serves as a barrier between the blood and the tissues of vessels, allowing metabolic regulation and the control of contraction and relaxation of smooth muscle through the release of various substances.

VI The oscillations around 0.007 Hz, apparently corresponds to NO-independent (probably prostaglandin-dependent) endothelial activity.

The differentiation of the oscillatory processes (as described above) will be exploited greatly in the following discussion. For visual representation of the intervals, one can refer to the analysis of blood flow signal presented on Figs. 4.14, 4.11a.

4.2 The Effect of Time-Varying Respiration on Cardiovascular System and Sympathetic Nerve Activity

4.2.1 Introduction

Time-variability and modulations are inherent part of the physiological oscillatory dynamics. One of the most pronounced and early discovered modulation is the respiration sinus arrhythmia, which describes how the breathing patterns modulate the heart rate [6, 7]. Modulations and time-variability investigated in different contexts [8–10], have also shown that their study can be useful in understanding of many physiological processes, their functioning and their existing relationships.

The objective of this investigation is to determine the effect of a deterministically varied respiration frequency on human oscillatory processes. The analysis will attempt to uncover how these processes are coordinated and how they influence each other. The time-variability of the respiration frequency is introduced externally, in a predefined procedure known to the investigator—thus in this way *deterministic non-autonomous influences are introduced* to the oscillatory dynamics. The controlled variability of the respiration is performed in order to study specifically how the varying respiration affects other processes, but also to use the perturbation for identifying existing relations and physiological mechanisms.

With its main function to provide oxygen, the respiration is one of the central processes in the human body. As such, it has attracted a lot of attention in physiology [11]. The relationship of respiration to heart rate variability has been identified as respiration sinus arrythmia [6]. Several studies have investigated how the sympathetic nerve activity is affected by different modes of breathing [10, 12, 13]. Of special interest is the study of low frequency components and sympathetic nerve activity [14], which also has been analyzed previously in conjunction with blood flow measurements [15]. Saul et al. have studied sympathetic nerve activity and haemodynamic signals under randomly varied breathing processes [16]. However, they did not studied the time-variability, the low frequency components are also not well localized, and the sympathetic nerve activity is not acquired by direct measurements of the nerve activity.

The following reports wavelet phase coherence analysis and information-theoretic approach for the detection of coupling between muscle sympathetic nerve activity and haemodynamic signals under deterministic time-varying perturbation of the respiration frequency. Wavelet phase coherence allows high resolution characterization of coherence i.e. coordination of the oscillatory dynamics at both high and low frequencies. The information-theoretic method quantifies the inter-oscillatory influences and reveals existence of causal relationships. All of the proposed techniques were able to trace (and to quantify statistically) the dynamical behavior and the time-variability, and to assess the time-domain information in accordance with the time-varying ramp perturbation. The main task was to investigate how the deterministic time-varying respiration regulates the neural and haemodynamic processes, and how this affects the causal inter-oscillatory relationships.

4.2.2 Measurements, Subjects and Signals

The total number of subjects analyzed was thirteen, and none of which smoked, had evidence of heart disease or took medication. The length of the recordings had mean of 72.3 min and standard deviation of 11.5 min. The minimum length was 53.4 min. There were two types of ramped paced breathing—first with gradually decreasing frequency (fast-to-slow) and second with gradually increasing frequency (slow-to-fast). Each recording contained several segments, with spontaneous breathing and then followed by several ramp breathing segments—the order and duration of all ramps is presented in Appendix D. The segments between the ramps were not analyzed because of the transient effect of the previous perturbation [17]. The mean length of spontaneous breathing segments was 7.9 min, with standard deviation of 2.6 min and a minimum of 6 min (which allowed the wavelet analysis to trace low frequencies down to 0.021 Hz). The ramps had lengths of approximately 9 min, with mean 9.05 and standard deviation of only 0.14 min.

The subjects were asked to breath voluntarily in accordance to a sine wave signal with time-varying frequency, which was shown on visual screen in front of them. In this way, the frequency of their respiration was varied with time.

The recordings included: electrocardiogram (ECG), blood pressure (BP) and carbon dioxide (CO_2) concentration signals. From the ECG signal a heart rate variability (HRV) signal was derived through marking of the R-peaks and linear interpolation between the consecutive time differences (for details see e.g. [3]). Similarly, the diastolic and systolic blood pressures were derived from the blood pressure signal. The recording also included the relatively rare and delicate measurement of muscle sympathetic nerve activity (MSNA). A multifiber sympathetic efferent traffic was measured invasively from the peroneal nerve muscle using microelectrodes with uninsulated tip diameters of about 2 μm. The sampling frequency of the recordings was 500 Hz.

4.2.3 Methods

This section briefly outlines the methods used for the analysis of the recordings. Statistical tools that are needed for the group statistical analysis are presented as well.

Wavelet Transform

The nature of the perturbation, where the frequency of the respiration was varied with time, means that the wavelet transform and its ability to trace the time-frequency dynamics was the optimal choice for analysis of the underlying oscillatory processes [5]. The method based on the continuous wavelet transform projects the signal from

time- to time-frequency domain with logarithmic frequency resolution [18]. Due to the adjustable length of the mother wavelet, the wavelet transform provides good frequency resolution, and by allowing time-localization, it improves upon Fourier transforms, which are based on fixed window lengths.

The wavelet transform enables one to derive the frequency content continuously in time by use of wavelets windows with variable length. A wavelet is shifted along the signal and a coefficient is calculated representing the strength of correlation between the signal and the wavelet. For the following analysis a Morlet mother wavelet was used:

$$\nu(u) = \frac{1}{\sqrt[4]{\pi}} e^{-i2\pi f_0 u} \cdot e^{-u^2/2},$$

where the central frequency was set to be $f_0 = 1\,\text{Hz}$. To create various scales of the wavelet comparable to the original signal, the mother wavelet is stretched and compressed by scaling factor s:

$$\Psi_{s,t}(u) = |s|^{-1/2} \cdot \nu\left(\frac{u-t}{s}\right). \tag{4.1}$$

In order to reach logarithmic resolution for the frequency, the scale factor s is increased exponentially. The transform itself is then a convolution of the wavelet and the original signal:

$$W(s,t) = \int_{-\infty}^{\infty} \bar{\Psi}_{s,t}(u) \cdot g(u) du, \tag{4.2}$$

where the $\bar{\Psi}$ represents the complex conjugate of Ψ. Thus any specific scale is avoided and the analysis becomes scale-independent in terms of frequency. The energy density in the time-scale domain is evaluated from the wavelet transform, and the wavelet power within the $f_1 : f_2$ frequency range can be calculated as:

$$\varepsilon(f_1 : f_2) = \int_{1/f_2}^{1/f_1} \frac{1}{s^2} |W(s,t)|^2 ds.$$

For the calculation of the transform the signals were re-sampled to 10 Hz, and their spectra below the lowest frequency analyzed (0.021 Hz for the segments and 0.0095 Hz for the whole signals) were removed by moving average technique. Use of longer wavelets for low frequency components, resulted in having higher wavelet amplitudes for the low compared with high frequencies. Due to this effect the low frequency oscillatory components are easily identified and traced. When one needs to detect the actual strength of particular frequency component, the wavelet spectral power is calculated.

Wavelet Phase Coherence and Windowed Wavelet Phase Coherence

By investigating the phase relationships, the wavelet phase coherence can determine the coordinating relationships between two signals. When inferring the relationships between signals with different or very low powers, a big advantage of the wavelet phase coherence is that it can detect significant coherence. This is particularly meaningful for low-frequency components, which make important, but not necessarily large contributions to total power.

The wavelet transform using Morlet wavelet is described as a complex function. This allows for the instantaneous phases of the signals to be analyzed directly from the transform. The latter was used for calculation of the respective phase difference and thus for evaluation of the phase coherence. It gives normalized measure of coherence ranging between 0 and 1.

Due to the complex nature of the Morlet wavelet, the wavelet transform for each time t_n and scale s_k, consists also of complex values:

$$W(s_k, t_n) = W_{k,n} = a_{k,n} + ib_{k,n}.$$

From here the instantaneous phase can be determined as the angle variable $\phi_{k,n} = arctan(b_{k,n}/a_{k,n})$. To evaluate the wavelet phase coherence, the respective phase difference $\Delta\phi_{k,n} = \phi_{2k,n} - \phi_{1k,n}$ is calculated [19]. To get normalized measure of coherence between 0 and 1, the sine and cosine of the phase difference are averaged in time, yielding the phase coherence function:

$$C_\phi(f_k) = \sqrt{\langle \cos(\Delta\phi_{k,n})\rangle^2 + \langle \sin(\Delta\phi_{k,n})\rangle^2}\,.$$

In order to follow how the phase coherence is varying with time, a windowed wavelet phase coherence can be calculated. A window is slide along the data in time domain and the phase coherence is evaluated and plotted as function of both frequency and time: $C_{W\phi}(f_k, t_k)$—with window of given size centered on a particular time t_k. The window size is varied for low to high frequencies in the same manner as the wavelet transform was calculated. In this way the same logarithmic scale for the frequency is preserved. On the end, each windowing is normalized by the particular window size, so that the measure returns normalized phase coherence between 0 and 1. Due to the finite length of the windows on the end of the sliding—there is a cut-off of information, and the corresponding plot has goblet-like shape. Detailed description of the method and its significance for adaptive windows is discussed in [20].

Coupling Between Interacting Oscillators: An Information-Theoretic Approach

An information-theoretic method proposed by Paluš & Stefanovska [21] was used for analysis of directionality of couplings and influences between weakly coupled

oscillatory processes. The method has prove to be useful in number of technical and physiological studies [22–24].

For inferring causality relationships i.e. directionality between two oscillatory processes, it estimates the 'net' information about certain time units in the future of the first process contained in the second process itself, by using an information-theoretic tool known as conditional mutual information. The two resultant conditional mutual information quantify the significant influence from the first to the second, and from the second to the first oscillatory signal. The influence that has the larger strength determines the predominant direction of coupling.

The information-theoretic method for quantification of couplings is based on conditional mutual information between the first $X_1(t)$ and the second $X_2(t)$ signal. The conditional mutual information is estimated as net information about the τ time units in future of the first signal $X_1(t)$ contained in the second signal $X_2(t)$ itself. First the τ increments are defined:

$$\Delta_\tau X_1 = X_1(t+\tau) - X_1(t).$$

Then the conditional mutual information i.e. the coupling of the first to second signal is defined as:

$$I_{21} = I(X_2, \Delta_\tau X_1 | X_1) = H(X_2|X_1) + H(\Delta_\tau X_1|X_1) - H(X_2, \Delta_\tau X_1|X_1),$$

where $H(x|y)$ and $H(x, y|z)$ are the conditional entropies defined in usual Shannonian sense. Similarly the coupling I_{12} from the first to the second signal is defined. The conditional mutual information I_{12} and I_{21} can be calculated by simple box-counting algorithm based on equiquantal marginal bins.

By applying the method one can infer the causality relationships between the signals, quantifying both the total influences and their time-variability by windowing the measure. Thermodynamically open systems and interacting physiological processes often can be mutually (bi-directionally) coupled, therefore it made sense to analyze not only the dominant direction, but also the two separate influences and their time-variations. The number of equiquantal bins used was $N = 4$, time shifts were taken from 5:50 and re-sampled signals to 10 Hz in normalized state space were used.

Statistical Analysis

Many data sets were not distributed normally (Kolmogorov-Smirnov test), so only medians, individual values and ranges were analyzed. A non-parametric statistical test was used, together with these quantities, to identify significant coherence, couplings and changes due to the time-varying ramped breathing.

The evaluation of the wavelet transform using different window lengths decomposed the signal into independent observations of particular frequency oscillations. The logarithmic scale for the spontaneous and ramped breathing segments (0.021–2 Hz) was divided into 95 independent segments for statistical analysis.

For the statistical investigation of changes in the wavelet power introduced by the ramped breathing, a non-parametric rank sum test on the individual wavelet powers was conducted. The significant segments were denoted as red vertical lines plotted between the two medians. Wherever a contiguous range of frequencies show a significant effect these lines are confluent, forming red areas. Additionally, the fixed frequency ranges for the oscillatory intervals (as described in Sect. 4.1.4) were tested for significance. Their significance was plotted with red asterisks.

When analyzing relationships between oscillatory processes in terms of wavelet phase coherence and coupling directionality, special care is needed. Namely, there can exist small non-zero values of the measures, even when in reality there are no real relationships. To overcome this discrepancy and to determine the statistical significance, a surrogate statistical analysis was performed. Amplitude-Adjusted Fourier transform (AAFT) surrogate signals were generated by shuffling the phases of the original time series to create new time series with the same means, variances, autocorrelation functions (and therefore, the same power spectra) as the original sequences, but without their phase relations [25, 26]. The average was calculated for 100 measures (phase coherence or couplings) calculated from 100 surrogate realizations of the signals. The phase coherence and coupling direction were considered to be statistically significant if their values were above the surrogate threshold, which was determined as the mean plus two standard deviations of the surrogate realizations.

When evaluating the wavelet phase coherence, the low-frequencies are represented with fewer periods than the high-frequency components. Consequentially, less variation of phase differences occurs at low-frequencies, and this is reflected in higher coherence values for low than high frequencies. The significant coherence of separate frequency segment was denoted with red area, and the significant ranges with red asterisks. A paired signed rank test was used for comparison of the measures with the surrogate threshold values. For visual inspection of the time-varying couplings only the values above the surrogate threshold were considered as significant. For quantification, the paired signed rank test was performed on the whole segment (spontaneous and ramp breathing) length. In all statistical tests, $P < 0.05$ was considered significant.

4.2.4 Results: Wavelet and Information-Theoretic Based Analysis

The main results of the individual and group analysis are presented in this section. Three subsections encapsulate the results in conceptual groups.

Oscillatory Dynamics

Figure 4.1 shows recordings made from one subject during spontaneous breathing at the beginning and the following ramp breathing. The carbon dioxide concentration recording presents the gradual frequency decrease of the breathing oscillatory

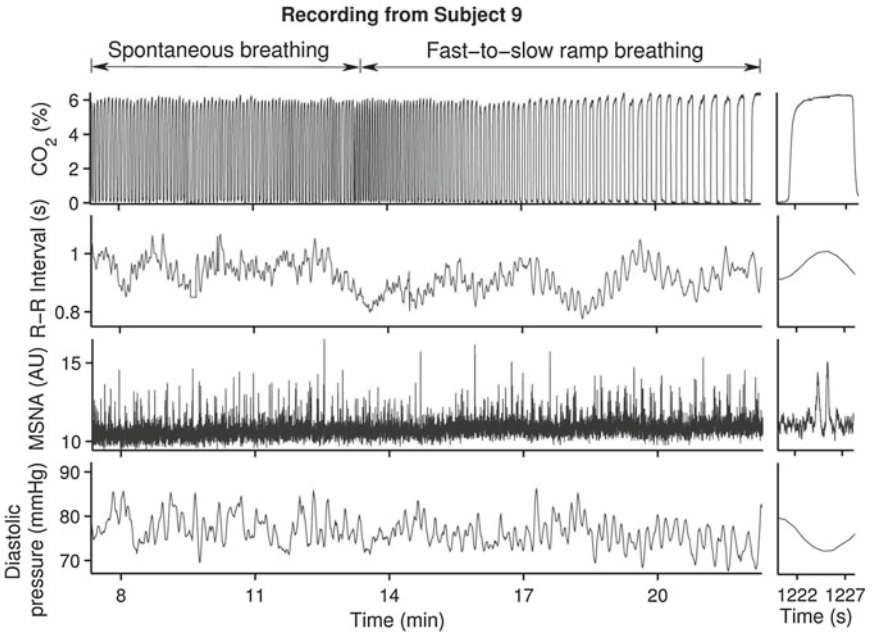

Fig. 4.1 Recording during spontaneous and first ramped breathing from Subject 9. During the first 6 min the subject breathed spontaneously, while in the following 9 min the breathing was gradually decreasing from fast to slow

process. The respiratory imprints are easily noticeable on the R-R interval and the diastolic pressure signal. Low frequency oscillations are also present in these signals. Muscle sympathetic nerve activity occur as groups of narrow bursts, which seem to appear in coordination with carbon dioxide cycles and are the most conspicuous for the slow breaths within the ramp segment. The enlarged time segments within one cycle of the carbon dioxide are presented on the right of the figure.

Figure 4.2 shows a wavelet transform of carbon dioxide concentration signal from one subject. With the ability to trace the time-frequency domain, the wavelet transform clearly demonstrates the time-varying nature of the ramp perturbation (note that the lines parallel to the ramped breathing are only their higher harmonics). During spontaneous segments the subject breathed freely and the wavelet amplitude is represented over a wide range of frequencies. The controlled ramp breathing sharply confined the wavelet amplitude around the time-varying frequency bands introduced deterministically by the perturbation.

The wavelet transform of muscle sympathetic nerve activity and its corresponding wavelet power from one subject are shown on Fig. 4.3. The influence of the respiration on the muscle sympathetic nerve activity is revealed by the presence of the ramp frequency content (compare the frequency components and the time-variability during spontaneous and ramp segments). The wavelet power demonstrates that the

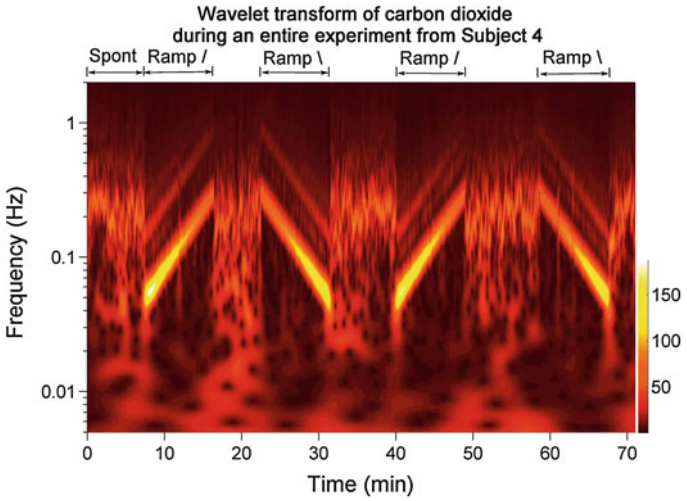

Fig. 4.2 Wavelet transform of carbon dioxide from Subject 4. The *contour plot* shows the wavelet transform for the whole duration of measurements. It is easy to notice the spontaneous breathing and the four (9 min) epochs of ramp breathing, which intermittently change from slow-to-fast to fast-to-slow. The wavelet amplitude during the spontaneous breathing is spread across various frequency bands, while during the ramped breathing the amplitudes are more concentrated around the ramping frequency

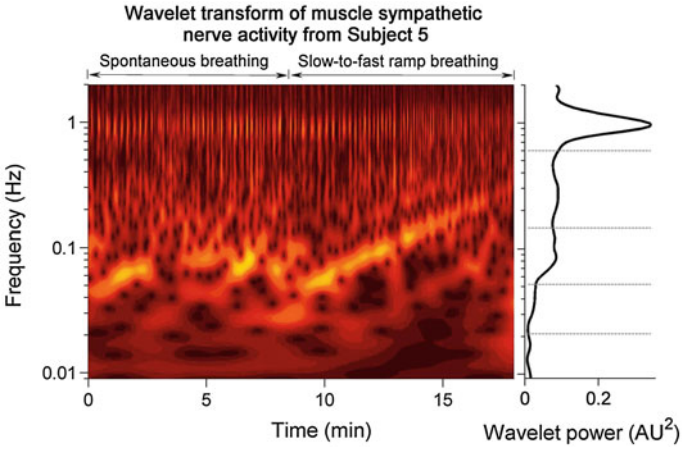

Fig. 4.3 Wavelet transform for muscle sympathetic nerve activity from Subject 5. The *left contour plot* shows the wavelet transform for the spontaneous breathing (8.5 min) and the slow-to-fast ramped breathing (9 min). The wavelet amplitudes on lower frequency (around and below 0.1 Hz) during the spontaneous breathing are changed due to the ramped breathing, making them dense around the controlled breathing frequency. The time-averaged wavelet power, plotted on the *right*, demonstrates that the strength of the higher frequency (around 1 Hz) is the highest, while the low frequencies are spread over the ramping bands

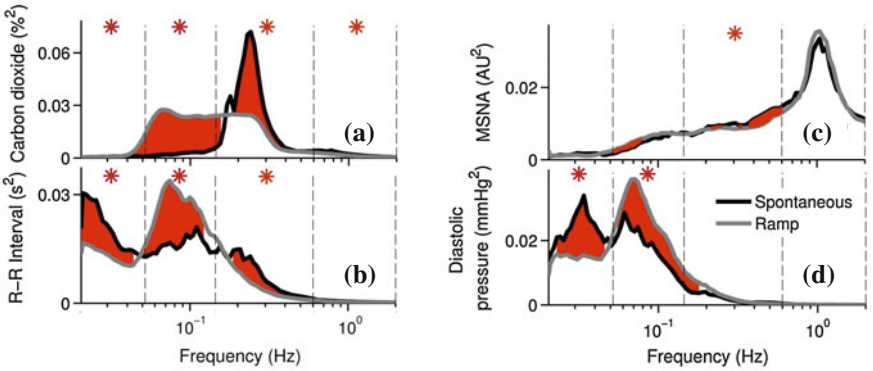

Fig. 4.4 Median wavelet power spectra of spontaneous (*black*) and ramped (*grey*) breathing segments. The figure shows how the time-varying breathing affected (**a**) the wavelet power spectra of carbon dioxide (**a**), R-R interval (**b**), muscle sympathetic nerve activity (**c**) and diastolic pressure (**d**). The *red areas* indicate significant change of individual wavelet powers, while the *red asterisks* show the significant range change. The perturbation that changed significantly the carbon dioxide, also significantly affected the R-R interval and the diastolic pressure at ramp and lower than ramp frequencies. The muscle sympathetic nerve activity power was not affected greatly

predominant periodic oscillations are around 1 Hz, while the lower frequency components that have less power are spread around the ramp breathing frequencies.

Figure 4.4 compares the median wavelet powers for all subjects and segments during spontaneous (black lines) and ramped (grey lines) breathing. Red shaded areas indicate specific frequencies at which the effect from the ramped breathing is significant (as indicated, a non-parametric rank sum test was applied to wavelet powers at each of the 95 frequencies). The red asterisks indicate the significance of the ramp effect within frequency ranges. The large significant difference in wavelet powers of spontaneous and ramped carbon dioxide shown on Fig. 4.4a demonstrates the nature and the effect of the ramp perturbation. The wavelet powers for R-R interval (Fig. 4.4b) and diastolic pressure (Fig. 4.4d), show that besides the significant effect on the ramp frequencies (around intervals II and III), there is also a significant difference on very low-frequency bands (interval IV), which are outside the initial frequency range from the ramp perturbation. The ramp breathing had little effect on the wavelet power of muscle sympathetic nerve activity (Fig. 4.4c), which was significant only within the ramp frequencies.

Coordination and Phase Coherence

Wavelet phase coherence was used to identify and quantify how the oscillatory signals interact i.e. if they are coordinated on some frequency ranges. Figure 4.5a–d shows the time-averaged coherence for spontaneous breathing while Fig. 4.5i–l shows ramped breathing coherence. The red shaded area represents statistically significant phase

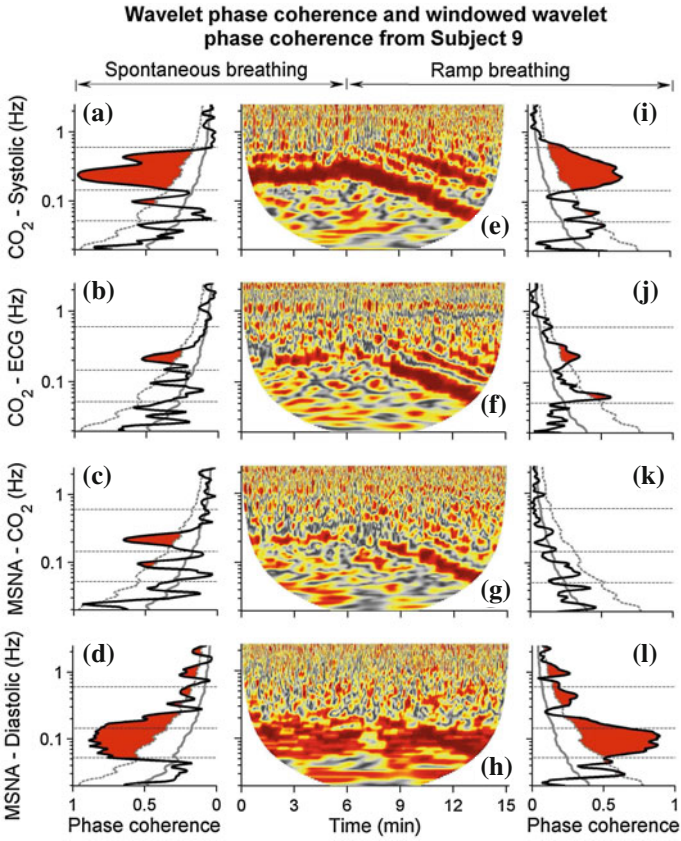

Fig. 4.5 Wavelet phase coherence and windowed wavelet phase coherence from Subject 9. The four contour (goblet-like) plots (**e**)–(**h**) show the windowed phase coherence for the first 15 (spontaneous 6 + ramp 9) min. One can easily notice the time-variability of the coherence from spontaneous to gradually changing during the ramp breathing. The plots (**a**)–(**d**) are for spontaneous, while (**i**)–(**l**) are for ramped breathing. The *red shaded area* represents the significant coherence above the surrogate threshold (mean plus two standard deviations), which is indicated by the *gray dashed line*. The implications of the coherence between the signals (as given on the left vertical axis-label) are discussed in more detail in the main text

coherence. Due to the time-varying nature of the ramp perturbation, windowed wavelet phase coherence was used to trace the time-variability of the coherence among ramp frequencies—Fig. 4.5e–h. The phase coherence shown on Fig. 4.5a, e, i, indicates that carbon dioxide and systolic pressure are highly and significantly coherent on breathing frequencies. The coherence was varying during the ramp breathing, following the frequencies introduced by the deterministic perturbation. Figure 4.5b, f, j represents the coherence between carbon dioxide and electrocardiogram (ECG) signal. The ECG signal was analyzed because it contains the 1 Hz oscillatory component of the heart activity. The relationship showed significant coherence only on

the breathing frequencies, which were affected during the ramp segment. The windowed wavelet phase coherence between muscle sympathetic nerve activity and carbon dioxide (shown on Fig. 4.5g) was not very high, and mostly it was concentrated around the breathing frequencies. During the ramp segment, this phase coherence was affected and spread across the ramp breathing frequencies. The latter resulted in lower and insignificant time-averaged coherence (Fig. 4.5k)—as opposed to the significant coherence during spontaneous breathing shown on Fig. 4.5c. Unlike the previous three relationships, the phase coherence between muscle sympathetic nerve activity and diastolic pressure was not qualitatively affected by the ramped breathing, and was relatively high at low frequencies. This was evident both from the windowed phase coherence Fig. 4.5h, and from the comparison of significant phase coherence in (Fig. 4.5d, cf. Fig. 4.5). The median phase coherence relationships were consistent with the individual presented on Fig. 4.5.

The effect from the ramp breathing on the relationships not directly connected with breathing, is presented on Fig. 4.6. Breathing does not affect the strong phase coherence that exists between diastolic pressure and muscle sympathetic nerve, and systolic pressure and R-R interval oscillations in low- and very low-frequency ranges (Panels A and B). However, breathing substantially augments phase coherence between systolic pressure and R-R interval oscillations at usual breathing frequencies (Panel B, red shading).

Couplings and Causal Relationships

Figure 4.7 shows the time evolution of carbon dioxide (grey) and muscle sympathetic nerve activity (black), and their respective coupling intensities (in both directions) from one subject. The red shaded areas indicate significant coupling above the surrogates threshold. The coupling intensities are an information-theoretic measure that

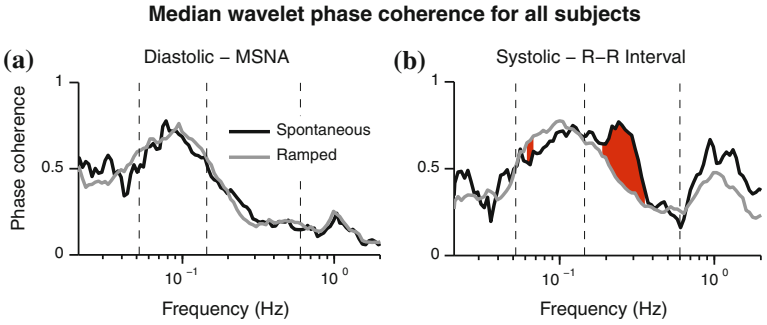

Fig. 4.6 Median phase coherence and the effect from the ramped breathing. Although neither breathing mode affected coherence between breathing and muscle sympathetic nerve oscillations (Panel (**a**)), breathing significantly increased phase coherence between systolic pressure and R-R interval oscillations in a limited range within the usual breathing frequency (Panel (**b**), *red shading*)

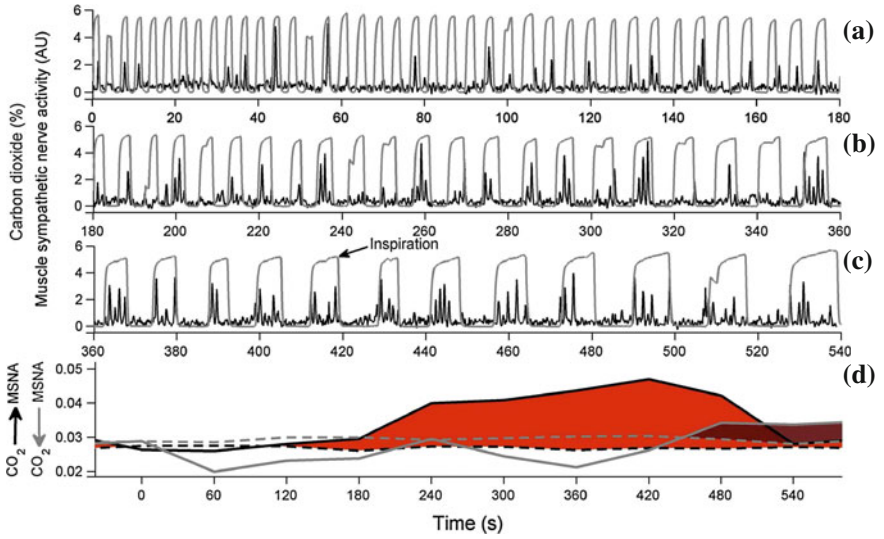

Fig. 4.7 Carbon dioxide and muscle sympathetic nerve activity, and their coupling during one fast-to-slow ramp from Subject 13. The three plots (**a**)–(**c**) show the time evolution of CO_2 (*gray*) and MSNA (*black*)—(**b**) continues after (**a**), and (**c**) after (**b**). The nerve bursts appear more coordinated with the high value of CO_2 as the ramp progress. **d** Shows the CO_2-to-MSNA coupling (*thick black*) and MSNA-to-CO_2 coupling (*thick gray*), and their surrogate thresholds with *dashed black* and *grey lines*, respectively. The *red shaded* areas represent the significant influences of the two directions. One can notice that the CO_2 influenced the MSNA more strongly and this coupling is increased as the ramped breathing progresses

quantifies the inter-oscillatory influences between carbon dioxide and muscle sympathetic nerve activity. The time-evolution of the signals during a ramp breathing shown on Fig. 4.7a–c demonstrate that muscle sympathetic nerve activity occurs as valleys of bursts appearing mostly during the inspiration cycle. As the ramp breathing progressed, the bursts appeared more frequently and in good coordination with the carbon dioxide cycles. The cause of the latter phenomenon is due to the coupling from carbon dioxide to muscle sympathetic nerve activity—as indicated on Fig. 4.7d. Namely, the intensities of the inter-oscillatory influences (shown on Fig. 4.7d) suggest that CO_2 to MSNA is the dominant direction, and its intensity becomes significant and increased as the ramp breathing progresses. The specific time-variability verifies the tight relationship between the influence of CO_2 on MSNA and the deterministic ramp perturbation.

Figure 4.8 presents the median and individual couplings between carbon dioxide and R-R interval, including the spontaneous (a and b), fast-to-slow (c and d) and slow-to-fast (e and f) ramp breathing segments. On the left plots (a, c and e) are the CO_2 to R-R interval, while on the right (b, d and f) the R-R interval to CO_2 couplings. The dashed black lines denote the surrogates' threshold. The P-value on each plot is evaluated within the whole segment between individuals, and

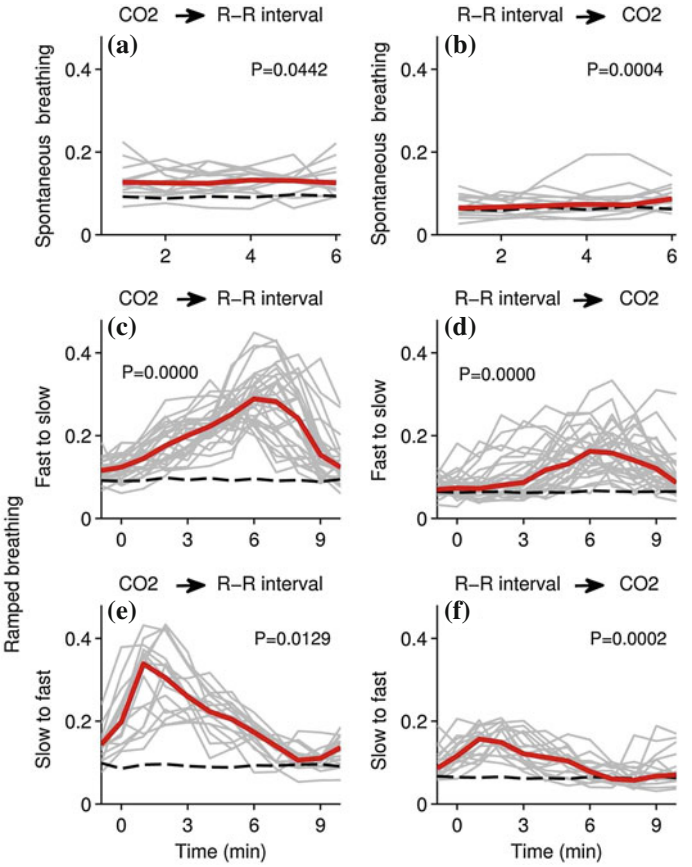

Fig. 4.8 Median (*red*) and individual (*grey*) couplings between carbon dioxide and R-R interval. On (**a**), (**c**) and (**e**) the CO_2 to R-R interval couplings are presented, while (**b**), (**d**) and (**f**) are showing the R-R interval to CO_2 couplings. The top two plots are for spontaneous, while the middle and bottom are for fast-to-slow and slow-to-fast ramped breathing. The dashed lines are the surrogate threshold (mean plus two standard deviations). During spontaneous breathing the couplings have almost constant values. The ramped breathing introduced time-variability and increased the influences towards low-frequencies. Overall the CO_2 to R-R interval couplings were more dominant

indicates if the coupling is significantly higher than the surrogates' threshold. During spontaneous breathing the couplings had almost constant values. The influence from CO_2 to R-R interval was the dominant direction. The ramped breathing enhanced the intensities of the couplings, and this effect was larger for low frequencies. The latter resulted in very clear time-varying imprint of the ramp perturbation (see e.g. Fig. 4.8c). These couplings had relatively large intensities, with CO_2 to R-R interval coupling having greater intensity and being the predominant direction.

4.2.5 Discussion

Simultaneous recordings from carbon dioxide concentration, muscle sympathetic nerve activity and haemodynamic signals were analyzed. The primary goal was to investigate how a deterministic time-varying respiration regulates and affects the oscillatory processes in cardiovascular and sympathetic neural system. Because their dynamics usually involve influence from several processes with diverse time-scales, which can be also time-varying, the time domain methods (such as time averages) are not appropriate for their analysis. Dynamical characterization (e.g. through wavelet based methods) on the other hand, offered better insight into the dynamics of the oscillators and the existing phenomena.

The advantage of measuring human subjects who can regulate the speed of their breathing voluntarily was used to introduce linearly increasing (decreasing) time-variability in the oscillators' dynamic. The wavelet analysis from CO_2 concentration (Fig. 4.2) showed how the perturbation confined the originally wide frequency range around the ramp frequency, and that the averaged wavelet power was significantly altered on all frequency intervals (Fig. 4.4a). The time-frequency representation demonstrated that at any frequency and time, the ramp perturbation can be determined consistently with the externally predefined variations.

The strong relationships between the respiration and heart activity, was observed in almost all of the performed analysis. The ramp breathing significantly altered not only the wavelet power at frequencies corresponding to the perturbation, but also the very low-frequencies [7], which were below the actual ramp breading frequencies (Fig. 4.4b). Figure 4.5 reveals that CO_2 and ECG are significantly coherent at breathing frequencies, probably due to the respiration sinus arrythmia modulation [6]. This phase coherence was following the specific time-varying breathing, and was enhanced for the lower frequencies of the ramping. The high intensities of inter-oscillatory couplings (Fig. 4.8) imply that there is high information flow between CO_2 and RR-interval signals. The results (Fig. 4.8) confirm and support the notion that respiration has a greater influence on the heart [21, 27, 28]. The ramp time-variability of the inter-oscillatory couplings pointed out that these causal relationships are more pronounced on lower breathing frequencies (see e.g. Fig. 4.8c, e).

The analysis of MSNA oscillatory [29] time-frequency content (Fig. 4.3) showed traces of the specific ramp breathing pattern, which at the same time did not exert a large effect on the averaged wavelet power (Fig. 4.4c). The phase coherence between MSNA and CO_2 was mostly concentrated around the breathing frequencies and during the ramp intervention it was significantly affected and spread around the ramp breathing frequencies Fig. 4.5. A simple time-domain observation (Fig. 4.7a–c) also suggests that MSNA appears as volleys of bursts within the CO_2 cycles [10, 11]. The cause of this phenomenon might be due to the coupling from CO_2 to MSNA, which was present throughout the ramp breathing and was significantly increased at low frequencies (in the same way as the bursts Fig. 4.7d).

The time-varying breathing also affected the diastolic and systolic blood pressure. The low frequency wavelet power of diastolic pressure was reduced outside the

ramped frequencies (Fig. 4.4d). The high phase coherence followed the respiration variations (Fig. 4.5). Interestingly, the phase coherence between sympathetic activity and diastolic pressure, and systolic pressure and R-R interval oscillations was high at low-frequencies, and was unaffected by the pattern of breathing (Fig. 4.6a, b). Contrariwise, phase coherence between systolic pressure and R-R interval oscillations (Fig. 4.6b) is augmented by spontaneous breathing, within a narrow portion of the usual breathing frequency range.

In summary, the time-varying breathing process significantly affected the functioning and regulation of several mechanisms in cardiovascular and sympathetic neural systems. In general, the gradually slower breathing provoked more 'information' flow, altered the coordination and increased the influences between the oscillatory processes. The manifestations and effects on this multi-coupled oscillatory system had the imprint of the particular form of the externally induced deterministic time-variation. The proposed analysis was able to detect, follow and statistically to quantify these features and phenomena.

4.3 Cardiorespiratory Interactions

In the previous section the effects from time-varying respiration were analyzed and statistically quantified on the whole group of measurements. The following discussion, first investigates more closely how the respiration with deterministic varying frequencies can affect the cardiorespiratory interactions i.e. how the ramped breathing affects the inherent dynamics and transitions between oscillatory processes of the heart and respiration. The cardiorespiratory interactions in relation to ageing are outlined shortly too. The Bayesian inferential technique (discussed previously in Chap. 3) is employed for the reconstruction of the interacting phase dynamics, and for evaluation of the qualitative states and transitions.

Before presenting the actual analysis, an important technical preprocessing issue is addressed. Namely, in order to infer the phase dynamics, one needs to have good estimate of the phases from the observable time-series. This is even more important when the oscillatory dynamics are time-varying and the analysis requires instantaneous phases. Potential difficulties for the phase estimation occur when the signals emanate from complex and/or mixed-mode oscillatory dynamics. Therefore, attention will first be spent on addressing some of the known methods for phase detection and the problems they hold, and an alternative approach for overcoming these issues will be proposed.

4.3.1 Instantaneous Phase Detection: Methods and Problems

The problem faced is to detect the phase at every moment in time from time-series containing oscillatory characteristics.[1] There exist two widely accepted methods for phase detection, which are used differently depending on the form of the signal.

The first method considers the interval between two well-defined events as a cycle, and that the phase increment between the events is exactly 2π. The procedure is similar to having a Poincaré cross section on the phase portrait of the attractor [30]. A cycle is described by only one information point while the intermediate points are linearly interpolated i.e. assigning the values of phase $\phi(t_k) = 2\pi k$ to the times t_k, and for arbitrary instant of time $t_k < \mathrm{t} < t_{k+1}$ the phase is defined as:

$$\phi_m(t) = 2\pi k + 2\pi \frac{t - t_k}{t_{k+1} - t_k}. \tag{4.3}$$

A detection of phase from an ECG signal (which has complex form), was used to present how the methods work. Figure 4.9a shows the ECG signal and the marked maxima t_k events. The instantaneous phase (Fig. 4.9 (b)). was estimated from the marked points and using Eq. (4.3).

The second method involves construction of the complex analytic signal $\zeta(t)$ [31] from a scalar experimental time series $s(t)$ via the Hilbert transform:

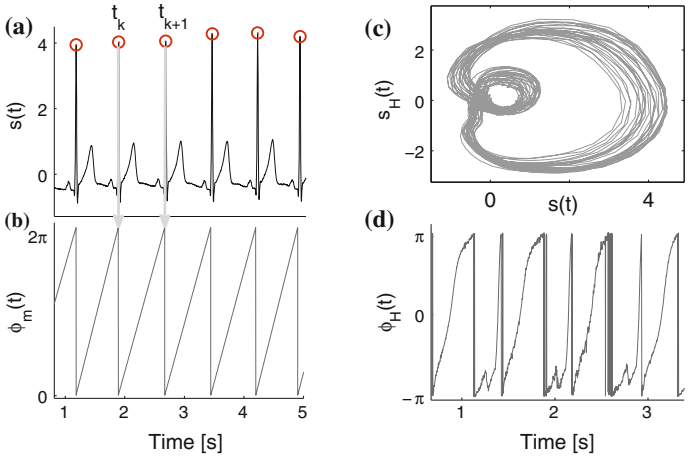

Fig. 4.9 Phase detection with marked-events and Hilbert transform methods. **a** ECG signal and marked maxima R-peaks. **b** The phase estimated as (4.3) using the peaks from (**a**). **c** The two-dimensional embedding using Hilbert transform of the same signal as **a**. **d** The spuriously detected phase using Hilbert transform (4.4)

[1] Note that instantaneous or 'every instant of time' in this context is finite and defined by the sampling frequency of the time-series.

$$\zeta(t) = s(t) + is_H(t) = A(t)e^{i\phi_H(t)}, \quad s_H(t) = \pi^{-1} P.V. \int_{-\infty}^{+\infty} \frac{s(\tau)}{t-\tau} d\tau, \quad (4.4)$$

where $s_H(t)$ is the Hilbert transform of signal $s(t)$. Hence, the angle variable $\phi_H(t)$ from the complex signal $\zeta(t)$ describes the required instantaneous phase. This approach is parameter free, very convenient for implementation, and if the signal is well defined and has narrow band spectra it gives phase information in every point of the time. However, if the two-dimensional embedding has loops or intersections this method will fail. In fact, due to its complex form with (P and Q) minor peaks between the maxima R-peak, the ECG signal is one such example. This is illustrated on Fig. 4.9c where the Hilbert transform embedding show clear folding and intersection. Thus the detected instantaneousness phase will be spurious Fig. 4.9d.

In studies of cardiorespiratory interactions, the phases from the respiration signal usually are estimated with Hilbert transform, while the ECG phase is detected through the marked events technique [3, 32]. This approach works well enough for observing dynamical behaviour which is longer than several oscillatory cycles, and where having only few phase information is enough (for example phase synchronization with synchrograms). But if one tries to infer the inherent oscillatory dynamics from complex signals, such as the coupling function and intrinsic time-varying parameters, then there is a need for instantaneous phase that contains more information of the cycle. For example, for cardiorespiratory interactions the ECG phase from the marked-events method contains only one information event per cycle, while the rest is simple interpolation. Alternatively, the Hilbert phase is not correctly detected either. Hence, there is a need for a phase estimate from complex signals that describes the phase (time-variability) at every instant in time.

Additionally, care must be taken when the signals contain parts and modulations from other (oscillatory) processes. In such cases, a preprocessing in terms of de-trending, filtering or decomposing is required. This will allow for interactions to be studied on self-sustained oscillatory processes with their own fundamental frequency. For example, the respiration signal might contain components from the heart activity, and if they are not taken into account, one might end up investigating synchronization between the heart and the influence from the heart on respiration [33, 34]. This is clearly wrong since the components are artifacts from the measuring procedure rather than the oscillatory dynamics of respiration, and the dynamics are coming from the same (cardiac) oscillator.

4.3.2 Instantaneous Phase Detection from Complex Mixed-Mode Signals

Recent development of techniques for decomposition of mix-mode signals has lead to the synchrosqueezed wavelet transform [35]. This method aims to decompose the signal into intrinsic mode components which can have time-varying spectrum. The transform is a combination of the wavelet transform and a special case of reallocation

method which tries to "sharpen" the time-frequency component $R(t, \omega)$ by allocating its value to a different point (t', ω') in the time-frequency plane, determined by the local behavior of $R(t, \omega)$ around (t, ω). It is based on wavelet transform $W(s, t)$, as described previously by Eqs. (4.1) and (4.2), which gives a time-scale representation of the frequency content that is spread out in s, but its oscillatory behavior in t are located around the original frequency ω, regardless of the value of s.

The synchrosqueezed transform aims to 'squeeze' the wavelet around the intrinsic frequency in order to provide better frequency localization. For any (s, t) for which $W(s, t) \neq 0$, a candidate instantaneous frequency for the signal g can be calculated as:

$$\omega_g(s, t) = -i \frac{\frac{\partial}{\partial t} W_g(s, t)}{W_g(s, t)}. \tag{4.5}$$

The information from the time-scale plane is transferred to the time-frequency plane, according to a map $(s, t) \rightarrow (\omega_g(s, t), t)$, in an operation called synchrosqueezing. The synchrosqueezed wavelet transform is then expressed as:

$$T_g(w, t) = \int_{A(t)} W_g(s, t) s^{-3/2} \delta(\omega(s, t) - \omega) ds, \tag{4.6}$$

where $A(t) = \{a; W_g(s, t) \neq 0\}$, and $\omega(s, t)$ is as defined in (4.5) above, for (s, t) such that $s \in A(t)$. Defined in this way, the transform is invertible and the signal can be reconstructed after the synchrosqueezing:

$$g(t) = \Re \mathfrak{e} \left[C_\psi^{-1} \int_0^\infty W_g(s, t) s^{-3/2} ds \right], \tag{4.7}$$

where C_ψ^{-1} has a constant value which is calculated from the mother wavelet $C_\psi^{-1} = \frac{1}{2} \int_0^\infty \frac{\overline{\Psi(\xi)}}{\xi} d\xi$. For practical reasons, when dealing with time series the frequency variable ω and the scale variable s can be "binned", i.e. $W_g(s, t)$ can be computed only at discrete values s_k, with $s_k - s_{k-1} = (\Delta s)_k$, and the synchrosqueezed transform $T_g(\omega, t)$ can be likewise determined only at the centers ω_l of the successive bins $[\omega_l - \frac{1}{2}\Delta\omega, \omega_l + \frac{1}{2}\Delta\omega]$, with $\omega_l - \omega_{l-1} = \Delta\omega$. The integral is written in this discrete form as the summation of different contributions, and Eq. (4.7) becomes:

$$g(t) = \Re \mathfrak{e} \left[C_\psi^{-1} \sum_k W_g(s_k, t) s_k^{-3/2} (\Delta s)_k \right] = \Re \mathfrak{e} \left[C_\psi^{-1} \sum_k T_g(\omega_l, t) (\Delta\omega) \right]. \tag{4.8}$$

Due to the good frequency localizations and invertibility, the synchrosqueezed wavelet transform can be used as an appropriate tool for identification and extraction of intrinsic oscillatory modes in time domain [35]. Moreover, the complex nature of the synchrosqueezed transform allows one to extract the phase of non-harmonic signals, or of some of their modes. The instantaneous phase can be calculated as the angle of the synchrosqueezed wavelet transform:

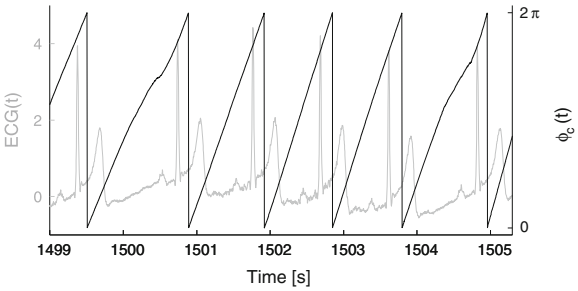

Fig. 4.10 Instantaneous phase detection from ECG signal, using the synchrosqueezed wavelet transform. The ECG signal is shown with *grey line*, and the phase $\phi_c(t)$ with *black*

$$\phi_l(t) = \angle\left[\sum_k T_g(\omega_l, t)(\Delta\omega)\right]. \tag{4.9}$$

The transform's great potential lies in its ability to determine instantaneous characteristics from signals with non-harmonic waveform [36]. The robust implementation and the visual time-frequency representation offer a convenient way for identification and analysis of mixed-mode oscillatory dynamics [37].

Figure 4.10 presents a specific application of the technique as a response to the originally posed question of how to detect reliably the instantaneous phase from ECG signal. One can notice that the phase was detected correctly in respect of the 2π cycles defined by the R-peaks, and that time-variability within the cycle is traced appropriately. It is worth noting that the ECG phase detected in this way (with instantaneous values) can be used appropriately by the Bayesian technique for inference of properties like coupling functions.

Exploiting the decomposition property of the transform, the phase can be detected only for certain specific oscillatory modes. For example the cardiac phase can be detected only from the intrinsic mode within the cardiac interval (Table 4.1), thus at the same time, a preprocessing procedure for removal of undesired modulations will be performed.

On the other hand, there exist cases where the modulations and external oscillatory premises can actually be used for further analysis. The latter can be even more important if the oscillatory mode is not directly measurable. For example, the blood flow signal measured with laser Doppler flowmetry (LDF), contains information about the blood propagations which are modulated by several oscillatory components. The activity within these frequency intervals, as elaborated in Table 4.1, can be decomposed and used for other analysis. Figure 4.11a shows the synchrosqueezed wavelet transform from human blood flow signal (also given by the wavelet transform and time-averaged wavelet power on Fig. 4.14). It is easy to notice the oscillatory modes in the corresponding frequency intervals (separated by dashed lines). This subject had very low respiratory influence on the blood flow processes. By applying the proposed technique, the oscillating processes were decomposed Fig. 4.11b–g and

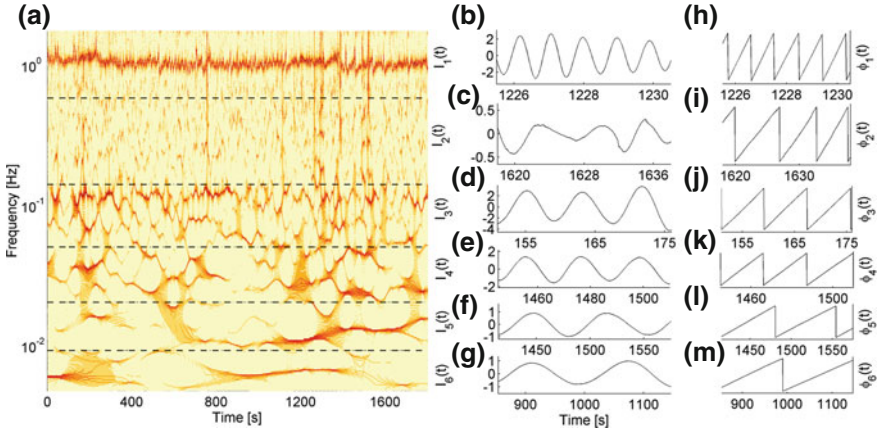

Fig. 4.11 Synchrosqueezed wavelet transform (**a**) from human blood flow signal. The oscillatory components as explained by Table 4.1 are separated by *black dashed lines*. The decomposed time-evolution (**b**)–(**g**) and their instantaneous phases (**h**)–(**m**), of the respective oscillatory component as shown on the *left* in (**a**). For example (**d**) shows the myogenic signals and (**j**) its phase

their instantaneous phases were detected directly Fig. 4.11h–m. Within each interval, the modes were selected as the maximal energy components, preserving their frequency and amplitude time-variations. This novel facility gives the opportunity for further analysis to be performed—including, for example, inter-oscillatory interactions in terms of synchronization and directionality. These results will be even more important because not all of the underlaying oscillatory processes can be measured directly. The inter-oscillatory analysis can give deeper insight into the cardiovascular mechanisms and causal relationships, and are certainly worth pursuing in the future.

4.3.3 Cardiorespiratory Interactions and the Effect from Time-Varying Respiration

The cardiac and respiratory activity can be seen as two self-sustained oscillatory processes that interact with each other. This sections investigates the cardiorespiratory interactions under conditions when the breathing pace is perturbed deterministically in a linear (ramp) manner—as explained in Sect. 4.2. The instantaneous cardiac phase was estimated from the ECG signal by synchrosqueezed wavelet transform described by Eq. (4.9). Similarly the respiratory phase was extracted from the CO_2 concentration signal. In order to avoid the potential phase disturbances introduced by the synchrosqueezed transform, the two phases were processed in a protophase-phase [38].

The Bayesian framework for inference of phase dynamics (Chap. 3) was applied on a segment with fast-to-slow ramp breathing. The results are summarized in Fig. 4.12.

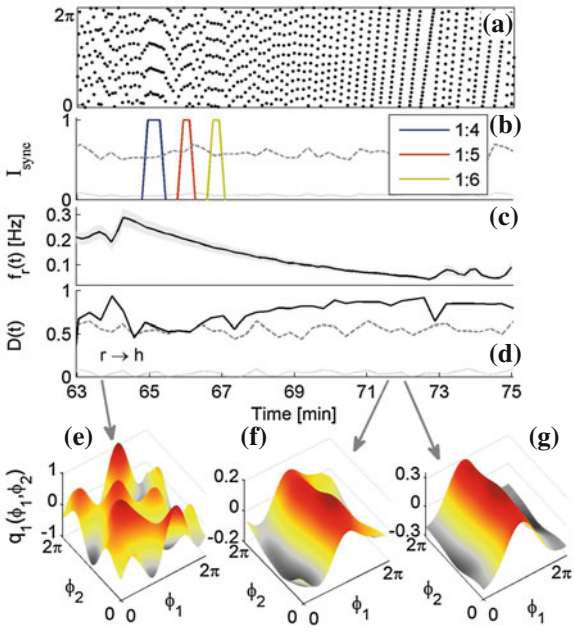

Fig. 4.12 Synchronization, directionality and coupling functions in the cardiorespiratory interaction. **a** Standard 1:*N* synchrogram. **b** Synchronization index for ratios 1:4, 1:5 and 1:6, as indicated. The *dashed line* represents the mean (*dotted*) +2 SD of synchronization indices from 100 surrogate [25] realizations. **c** The time-varying respiration frequency (note the downward ramp due to pacing). The *gray areas* on **c** represent ±2 SD from the mean value. **d** Directionality index: *the dashed lines* represent the mean (*dotted*) +2 SD of directionality indices from 100 surrogate realizations. **e–g** Coupling functions $q_1(\phi_1, \phi_2)$ calculated at different times, as indicated by the *grey arrows*. From [41] © (2012) by the American Physical Society

The inferred respiratory frequency shown on Fig. 4.12c demonstrates the ramped breathing variability. The secondary purpose for presenting the ramp is to follow the changes of other measures with respect to the perturbation applied. By normalizing the inferred coupling parameters, one can determine the net directionality of the interactions. Figure 4.12d suggests that the degree of directionality is time-varying, but confirms that respiration-to-heart is dominant [3, 28, 39, 40]. To determine whether cardiorespiratory synchronization exists in certain ratios, the set of inferred coupling parameters was used to reconstruct the torus map and for investigating whether the root $M(\psi_e) = \psi_e$ exists or not. Figure 4.12b shows the detection of transitions from the non-synchronized to the synchronized state, which in turn change in different ratios: 1:4 to 1:5 to 1:6, as the ramp progressed. The synchronization detection and the respective transitions were consistent with the respective synchrogram Fig. 4.12a. The surrogate testing on (b) and (d) was performed in order to refute the hypothesis that the measures happen by chance, and to determine the significance threshold.

The cardiorespiratory coupling function, evaluated for three different time windows indicated by the arrows, is presented on Fig. 4.12e–g. For simplicity and clarity only q_1 is shown (the qualitative behavior of q_2 was similar). The interactions are described by complex functions whose form changes qualitatively over time—cf. Fig. 4.12e with (f) and (g). The latter implies that the functional relation for the cardiorespiratory interactions is not a time-invariant function, but is in fact a time-varying process for itself. The time-evolution of the coupling functions is evident by analyzing consecutive time windows—cf. the similarities i.e. evolution of Fig. 4.12f, g. It is important to note that this variability is not caused by the ramp time-varying respiration frequency (which is decomposed separately), and that the phenomenon of time-evolving coupling functions was observed also on spontaneously breathing subjects.

The ramped breathing showed that the cardiorespiratory coordination depends and is regulated to a great extent by the respiration dynamics. The analysis indicated that the Bayesian technique detected the occurrence of transitions to/from synchronization and revealed details of the phase dynamics, thus describing the inherent nature of this transitions. It was found that the externally induced varying respiration acts as a cause for these qualitative transitions. Additional complexity for the interactions and their analysis was encountered by the coupling functions which were also time-varying processes.

4.3.4 Cardiorespiratory Interactions and Ageing

The Bayesian inference (presented in Chap. 3) can be quite useful in treating real-life problems. Its application for reconstruction of cardiorespiratory interactions can be used to study and quantify certain physiological states and diseases. This was already proven useful in a study about the evolution of human cardiorespiratory interactions in relation to ageing [41]. In the following, the main results are shortly reported and reviewed. The study describes an analysis of cardiac and respiratory time series recorded from 189 subjects of both genders, with age ranging from 16 to 90 years.

The phases were estimated using the wavelet synchrosqueeze decomposition from the ECG and the respiration signal. The Bayesian inference is applied to decompose the deterministic phase dynamics and the noise. After the time-varying parameters are decomposed, synchronization, directionality and coupling functions are studied and statistically assessed in relation to different age groups. The heart and respiratory coupling functions are further divided into three parts, representing: coupling-induced self-interaction; direct driving by the other system; and indirect interactions.

It was found that there is no significant correlation of the overall synchronization duration with age. It seems also that certain synchronization ratios may be characteristic of particular ages and genders. The commonest cardiorespiratory synchronization ratio was found to be 4:1. The overall influence of respiration on the heart decreases with age, while influence in the opposite direction stays constant, leading to a net decrease of coupling directionality with age.

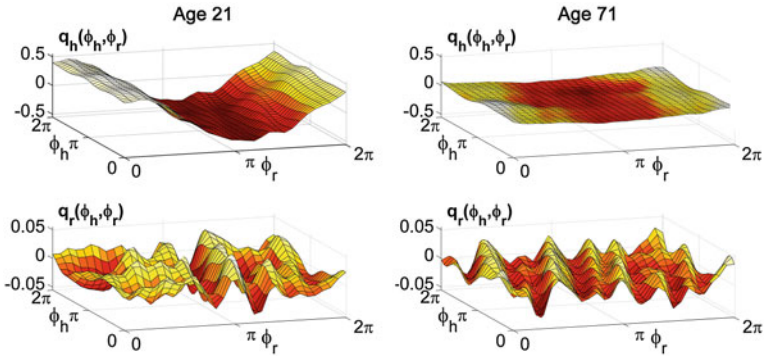

Fig. 4.13 Typical time-averaged coupling functions for a young (*left*) and an old (*right*) male subjects, aged 21 and 71 years respectively. The coupling function $q_h(\phi_h, \phi_r)$ represents the influence from respiration to heart, while $q_r(\phi_h, \phi_r)$ the influence from heart to respiration. From [42] © (2013) The Royal Society

To gain further insight into the nature of the cardiorespiratory interaction, the overall form of the reconstructed coupling functions is analyzed. Figure 4.13 shows the time-averaged versions of the coupling functions $q_{h,r}$ typical of a younger and an older subject. Decrease of the respiration sinus arrythmia amplitude with age can be seen by comparing Fig. 4.13a and b. The respiratory coupling q_r shown in (c), (d) seems to be quite irregular and not age dependent. Underlying all these separate effects, the heart coupling function q_h changes markedly with age, both in its average form and in its time-variability, whereas the respiratory coupling function seems to be irregular and unaffected by age.

4.4 Reproducibility of LDF Blood Flow Measurements: Dynamical Characterization Versus Averaging

In experimental analysis it is crucially important to have precise and reliable measurements. One of the tests for precision is reproducibility, which is the degree of agreement between measurements conducted on replicate conditions in different locations by different people. Recently, a question about the reproducibility of Laser Doppler Flowmetry (LDF) measure of blood flow was raised [42]. By means of determining cutaneous vascular conductance (CVC), the authors seek to evaluate reproducibility by averaging relatively short time segments of data during or immediately after some perturbation. They concluded that the reproducibility of measurements on the forearm is limited by spatial variability in the microvasculature.

This naturally raised the discussion if the analyzing methods used were appropriate for analysis of LDF blood flow signals, which have a mixed mode oscillatory nature. Another important issue raised was how to assess external (non-autonomous)

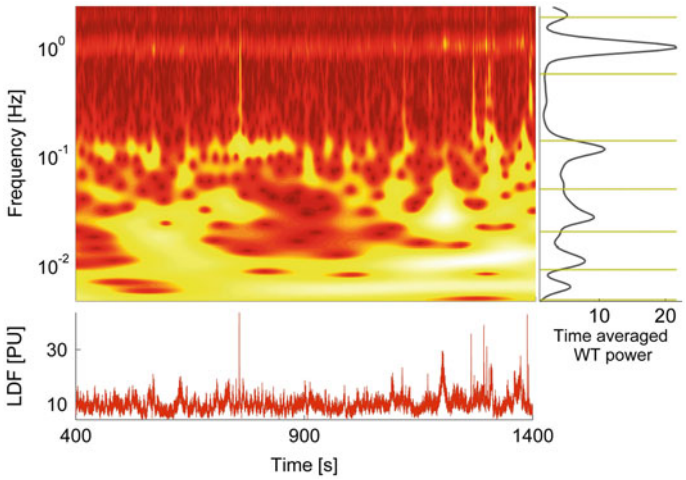

Fig. 4.14 Wavelet transform of LDF variability (*top left*), plotted above the raw signal in standard perfusion units (*bottom*) and the averaged wavelet power spectrum (*right*). The six frequency intervals as presented in Table 4.1 are indicated by *horizontal lines* and correspond (from the *top*) to: cardiac activity; respiration; myogenic oscillations; neurogenic; NO-related endothelial processes; and non-NO-related endothelial processes. From [17] © (2011) Elsevier

perturbations, the kind of discrepancy that can occur and how to analyze them properly. These two issues are presented in more detail below [17].

4.4.1 Blood Flow Analysis

The reproducibility of forearm LDF measurements was investigated in earlier work [43] by means of dynamical characterization of the oscillatory signals. It was established that the issue of spatial variability could be mitigated by careful placement of the sensors: good reproducibility was obtained by avoiding proximity to the larger vessels, hairs, and blemishes. It was found that this is true both for spatial reproducibility, with simultaneous measurements at different positions on the same arm, and for temporal reproducibility, with sequential measurements at the same position.

Time-averages measures are a standard tool for analysis in physiology. But the question raised is whether time-averaging provides a satisfactory method for characterising blood flow, developing LDF criteria, or testing LDF reproducibility. Since blood flow is inherently oscillatory in nature [4], averaging will inevitably produce variable results depending on how the window is positioned relative to the phase of an oscillation unless, of course, the window is very much longer than the oscillation period. In reality, the situation is even more complex because there is not just one oscillatory process in blood flow, but at least six [44]. Figure 4.14 shows a wavelet transform of typical LDF blood flow data. The slower of the two endothelial-related

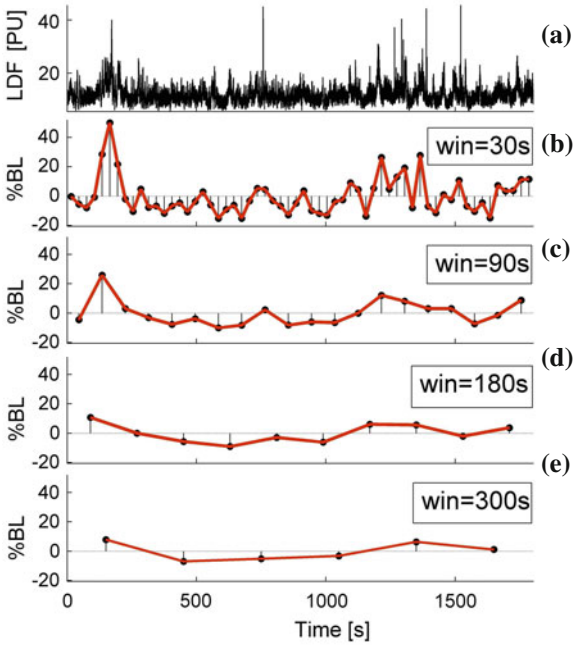

Fig. 4.15 The raw LDF blood flow signal from Fig. 4.14 averaged over successively larger window sizes, as indicated by the numbers in each box. From [17] © (2012) Elsevier

oscillations has a period of about 0.007 Hz, so that the averaging window would need to be much longer than 2.4 min in order to avoid irreproducibility from this source. One can in principle always achieve reproducibility of an LDF average by using a long enough averaging interval, or by averaging over a large enough spatial area but, in doing so, one inevitably throws away a lot of potentially useful information.

The dynamical characterization, on the other hand, prescribes that it is better to accept that blood flow is inherently oscillatory, and to frame the criteria for LDF reproducibility on that basis. Thus, rather than asking whether the average blood flow has changed over time or in spatial position, it will be better and more rewarding to ask whether the characteristics of the oscillations have changed, for example: their amplitudes and frequencies, which are already known to be reproducible in time and space; or the extent to which the different oscillations mutually interact and perhaps synchronize with each other. Changes in these quantities have been related successfully to several different pathological conditions e.g. congestive heart failure, hypertension and diabetes as well as to other states of the body like e.g. exercise and anaesthesia [44]. Even if averages could be measured reproducibly, they would do little to characterize or help diagnose these conditions.

To illustrate these points, Fig. 4.15 shows the same LDF segment as Fig. 4.14 and a series of time-averaged flux values made with different window sizes. If a short time is taken to "read" the value, the difference between readings can be as high as 60 %

of the baseline value. The longer the window is, the less variable the average value becomes. However, as shown in Fig. 4.14 there are distinct patterns in the variability that are missed if only the average is taken into account. Moreover, the patterns are visible on several different time-scales so that a relatively long recording time is needed to capture the dynamical properties of the blood perfusion signal. Thus, for analysis of LDF measurements, the dynamical description in terms of the parameter values characterizing the oscillations, can be more appropriate. In their response [45], the authors also add that both approaches: the time-averaging and dynamical characterizations are of interest, being different but complementary.

4.4.2 Numerical Study of Transient Effect on Interacting Oscillators Subject to Non-Autonomous Perturbations

In physiology, one of the standard procedures for investigating the mechanisms and existing relationships is to subject the systems to external perturbations. In this way the examiners can follow how the system reacts to this influence, and if there are some interactions with other systems which are affected by this perturbation. Obvious examples include the ramp breathing discussed in Sect. 4.2, local heating or post-occlusive reactive hyperaemia. Often several perturbations are performed consecutively, and in this particular case special care must be taken. When the systems are oscillatory processes, the transient response from the perturbations (if not treated well) can have an effect on the analysis and their reproducibility.

In a complex dynamical system such as the skin microvasculature, any perturbation is likely to involve nonlinear hysteresis effects. Figure 4.16 shows the results of a numerical simulation of just two coupled oscillatory processes subjected to repeated external perturbation. The model consists of bi-directionally-coupled limit-cycle oscillators (based on Poincaré oscillators), subject to external perturbations and weak noise:

$$\begin{aligned} \dot{x}_1 &= -\alpha_1(r_1 - a_1)x_1 - \omega_1(y_1 - \beta_1 r_1) + \varepsilon_1 x_2 + \xi_1(t) \\ \dot{y}_1 &= -\alpha_1(r_1 - a_1)y_1 + \omega_1(x_1 - \beta_1 r_1) + \varepsilon_1 y_2 + \xi_1(t) - s_1(t) - s_2(t), \end{aligned} \tag{4.10}$$

$$\begin{aligned} \dot{x}_2 &= -\alpha_2(r_2 - a_2)x_2 - \omega_2(y_2 - \beta_2 r_2) + \varepsilon_2 x_1 + \xi_2(t) \\ \dot{y}_2 &= -\alpha_2(r_2 - a_2)y_2 + \omega_2(x_2 - \beta_2 r_2) + \varepsilon_2 y_1 + \xi_2(t) - s_2(t), \\ r_i &= \sqrt{x_i^2 + y_i^2}; i = \{1, 2\}. \end{aligned} \tag{4.11}$$

The parameters were set to values mimicking the frequency spectra: cycle radii $a1 = a2 = 1$; frequencies $\omega_1 = 2\pi 0.1$, $\omega_2 = 2\pi 0.011$; couplings $\varepsilon_1 = 0.01$, $\varepsilon_1 = 0.001$; parameters for speed of convergence $\alpha_1 = 0.001, \alpha_2 = 0.1$ and

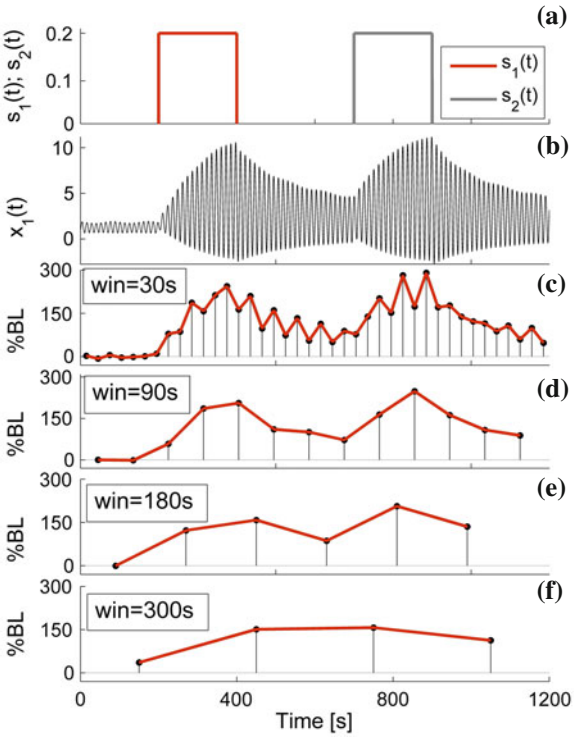

Fig. 4.16 The effect of repeated perturbations on the two-oscillator model described by Eqs. (4.10) and (4.11), showing the resultant changes in the mean value and transient effects as they are observed using different window sizes. From [17] © (2011) Elsevier

parameters for the center of rotation $\beta_1 = 0.4$ and $\beta_2 = 0.01$. The noise is white Gaussian, with zero mean $\langle \xi_i(t) \rangle = 0$ and correlation $\langle \xi_i(t)\xi_i(s) \rangle = D\delta(t-s)$, where D is the noise strength ($D1 = D2 = 0.003$). A long initial transient time (1000 s) was discarded and the stationary state was analyzed. The non-autonomous perturbations $s_1(t)$, $s_2(t)$ are simple step signals, each with length t = 200 s and amplitudes $s_{1H} = s_{2H} = 0.2$, as presented on Fig. 4.16a.

For the first 200 s, the first oscillator is unperturbed and its time-averages are around the baseline (except for small deviations due to weak noise and coupling). During the high value of $s_1(t)$ (t = 200–400 s) the first oscillator is perturbed and its time-averages are affected accordingly. It is evident that x_1 is then subject to the gradually decreasing after effect of the perturbation. This transient period (t = 400–700 s) appears because the oscillator needs a certain time to converge to its limit cycle. The length of the transient depends on the characteristics and the parameters of the oscillator. The associated time-averages are affected and the values are far from the baseline. A second perturbation (t = 700–900 s) involves perturbing both of the oscillators by $s_2(t)$. Note that, during this period, the first oscillator is subject

to the additional and indirect influence of the second oscillator, resulting in higher time-averages. After the second perturbation $s_2(t)$ finishes, the first oscillator is again left in perturbed state and only gradually returns towards its baseline value.

It is evident that transients in the oscillatory behaviour may persist for much longer than the timescale of the perturbation itself. Due to the coupled nature of the oscillatory processes, perturbing either oscillator results in the transient behaviour of both oscillators, leading to changes in the time-averaged values (which obscure the oscillations themselves). Repeated perturbations result in overlapping transient responses. Hence, when subjecting the microvasculature to a perturbation, care should be taken to understand the role of oscillatory processes: short-time average values may capture only a part of the transient physiological response.

References

1. E.N. Marieb, *Human Anatomy and Physiology*, 7th edn. (Benjamin Cummings, San Francisco, 2007)
2. B. Charlie, *Nervous System* (Mosby, Edinburgh, 2003)
3. Y. Shiogai, A. Stefanovska, P.V.E. McClintock, Nonlinear dynamics of cardiovascular ageing. Phys. Rep. **488**, 51–110 (2010)
4. A. Stefanovska, M. Bračič, Physics of the human cardiovascular system. Contemp. Phys. **40**, 31–55 (1999)
5. A. Stefanovska, M. Bračič, H.D. Kvernmo, Wavelet analysis of oscillations in the peripheral blood circulation measured by laser Doppler technique. IEEE Trans. Bio. Med. Eng. **46**(10), 1230–1239 (1999)
6. J.A. Hirsch, B. Bishop, Respiratory sinus arrhythmia in humans: how breathing pattern modulates heart rate. Am. J. Physiol. Heart Circul. Physiol. **241**(4), H620–H629 (1981)
7. T.E. Brown, L.A. Beightol, J. Koh, D.L. Eckberg, Important influence of respiration on human R-R interval power spectra is largely ignored. J. Appl. Physiol. **75**(5), 2310–2317 (1993)
8. L.J. Badra, W.H. Cooke, J.B. Hoag, A.A. Crossman, T.A. Kuusela, K.U.O. Tahvanainen, D.L. Eckberg, Respiratory modulation of human autonomic rhythms. Am. J. Physiol. Heart Circul. Physiol. **280**(6), H2674–H2688 (2001)
9. M.B. Lotrič, A. Stefanovska, Synchronization and modulation in the human cardiorespiratory system. Physica A **283**(3–4), 451–461 (2000)
10. V.G. Macefield, B.G. Wallin, Modulation of muscle sympathetic activity during spontaneous and artificial ventilation and apnoea in humans. J. Auton. Nerv. Syst. **53**(23), 137–147 (1995)
11. D.L. Eckberg, The human respiratory gate. J. Physiol. **548**(2), 339–352 (2003)
12. D.R. Seals, N.O. Suwarno, J.A. Dempsey, Influence of lung volume on sympathetic nerve discharge in normal humans. Circ. Res. **67**(1), 130–141 (1990)
13. P. Van De Borne, N. Montano, K. Narkiewicz, J.P. Degaute, A. Malliani, M. Pagani, V.K. Somers, Importance of ventilation in modulating interaction between sympathetic drive and cardiovascular variability. Am. J. Physiol. Heart Circul. Physiol. **280**(2), H722–H729 (2001)
14. A. Bernjak, J. Cui, S. Iwase, T. Mano, A. Stefanovska, D.L. Eckberg, Human sympathetic outflows to skin and muscle target organs fluctuate concordantly over a wide range of time-varying frequencies. J. Physiol. **590**, 363–375 (2011)
15. T. Soderstrom, A. Stefanovska, M. Veber, H. Svensson, Involvement of sympathetic nerve activity in skin blood flow oscillations in humans. Am. J. Physiol. Heart Circul. Physiol. **284**(5), H1638–H1646 (2003)
16. J.P. Saul, R.D. Berger, P. Albrecht, S.P. Stein, M.H. Chen, R.J. Cohen, Transfer function analysis of the circulation: unique insights into cardiovascular regulation. Am. J. Physiol. Heart Circul. Physiol. **261**(4), H1231–H1245 (1991)

17. A. Stefanovska, L.W. Sheppard, T. Stankovski, P.V.E. McClintock, Reproducibility of LDF blood flow measurements: dynamical characterization versus averaging. Microvasc. Res. **82**(3), 274–276 (2011)
18. G. Kaiser, *A Friendly Guide to Wavelets* (Birkhäuser, Boston, 1994)
19. A. Bandrivskyy, A. Bernjak, P. McClintock, A. Stefanovska, Wavelet phase coherence analysis: application to skin temperature and blood flow. Cardiovasc. Eng. **4**(1), 89–93 (2004)
20. L.W. Sheppard, A. Stefanovska, P.V.E. McClintock, Testing for time-localized coherence in bivariate data. Phys. Rev. E **85**, 046205 (2012)
21. M. Paluš, A. Stefanovska, Direction of coupling from phases of interacting oscillators: an information-theoretic approach. Phys. Rev. E **67**, 055201 (2003)
22. B. Musizza, A. Stefanovska, P.V.E. McClintock et al., Interactions between cardiac, respiratory and EEG-oscillations in rats during anaesthesia. J. Physiol. **580**(1), 315–326 (2007)
23. A. Porta, A.M. Catai, A.C.M. Takahashi, V. Magagnin, T. Bassani, E. Tobaldini, P. van de Borne, N. Montano, Causal relationships between heart period and systolic arterial pressure during graded head-up tilt. Am. J. Physiol.-Regul. Integr. Comp. Physiol. **300**(2), R378–R386 (2011)
24. K. Lehnertz, Assessing directed interactions from neurophysiological signals—an overview. Physiol. Measur. **32**(11), 1715–1724 (2011)
25. T. Schreiber, A. Schmitz, Improved surrogate data for nonlinearity tests. Phys. Rev. Lett. **77**(4), 635–638 (1996)
26. J. Theiler, S. Eubank, A. Longtin, B. Galdrikian, J.D. Farmer, Testing for nonlinearity in time series: the method of surrogate data. Physica D **58**(1–4), 77–94 (1992)
27. C. Schäfer, M.G. Rosenblum, J. Kurths, H.H. Abel, Heartbeat synchronised with ventilation. Nature **392**(6673), 239–240 (1998)
28. A. Bahraminasab, F. Ghasemi, A. Stefanovska, P.V.E. McClintock, H. Kantz, Direction of coupling from phases of interacting oscillators: a permutation information approach. Phys. Rev. Lett. **100**, 084101 (2008)
29. S.M. Barman, Sympathetic nerve activity has more character than you may think. J. Physiol. **587**(20), 4767–4768 (2009)
30. A. Pikovsky, M. Rosenblum, J. Kurths, *Synchronization—A Universal Concept in Nonlinear Sciences* (Cambridge University Press, Cambridge, 2001)
31. D. Gabor, Theory of communication. J. IEEE **93**, 429–457 (1946)
32. M.G. Rosenblum, A.S. Pikovsky, J. Kurths, Synchronization approach to analysis of biological systems. Fluctuat. Noise Lett. **4**(1), 53 (2004)
33. T. Stankovski, B. Musizza, P.V.E. McClintock, A. Stefanovska, Phase detection from the respiration signal, in *Proceedings of the 6th ESGCO, Berlin, Germany*, 2010
34. A. Stefanovska, P.V.E. McClintock, J. Ræder, A.F. Smith, *Nonlinear Dynamics of Anæsthesia: from Theory to Clinical Application* (Springer, Berlin, to be published)
35. I. Daubechies, J. Lu, H.-T. Wu, Synchrosqueezed wavelet transforms: an empirical mode decomposition-like tool. Appl. Comput. Harmon. Anal. **30**(2), 243–261 (2011)
36. H. Wu, Instantaneous frequency and wave shape functions. *arXiv:1104.2365v1*, 2011
37. E. Brevdo, N.S. Fuckar, G. Thakur, H. Wu, The synchrosqueezing algorithm: a robust analysis tool for signals with time-varying spectrum. *arXiv:1105.0010v1*, 2011
38. B. Kralemann, L. Cimponeriu, M. Rosenblum, A. Pikovsky, R. Mrowka, Uncovering interaction of coupled oscillators from data. Phys. Rev. E **76**, 055201 (2007)
39. M.G. Rosenblum, A.S. Pikovsky, Detecting direction of coupling in interacting oscillators. Phys. Rev. E. **64**, 045202 (2001)
40. J. Jamšek, M. Paluš, A. Stefanovska, Detecting couplings between interacting oscillators with time-varying basic frequencies: instantaneous wavelet bispectrum and information theoretic approach. Phys. Rev. E **81**, 036207 (2010)
41. D. Iatsenko, A. Bernjak1, T. Stankovski, Y. Shiogai, P.J. Owen-Lynch, P.B.M. Clarkson, P.V.E. McClintock, A. Stefanovska, Evolution of cardio-respiratory interactions with age. Phil. Trans. R. Soc. Lond. A. **371**, 20110622 (2013)

42. M. Roustit, S. Blaise, C. Millet, J.L. Cracowski, Reproducibility and methodological issues of skin post-occlusive and thermal hyperemia assessed by single-point laser Doppler flowmetry. Microvasc. Res. **79**(2), 102–108 (2010)
43. M. Bračič, A. Stefanovska, Wavelet based analysis of human blood flow dynamics. Bull. Math. Biol. **60**(5), 919–935 (1998)
44. A. Stefanovska, Coupled oscillators: complex but not complicated cardiovascular and brain interactions. IEEE Eng. Med. Biol. Mag. **26**(6), 25–29 (2007)
45. J. Cracowski, M. Roustit, Reproducibility of LDF blood flow measurements: dynamical characterization versus averaging. A response to the letter from Stefanovska. Microvasc. Res. **82**, 274–276 (2012)